

Liquid-infiltrated photonic crystals*

— enhanced light-matter interactions for lab-on-a-chip applications

Niels Asger Mortensen, Sanshui Xiao, Jesper Pedersen

MIC – Department of Micro and Nanotechnology, Nano•DTU, Technical University of Denmark, Ørstedes Plads, DTU-building 345 east, DK-2800 Kongens Lyngby, Denmark.

Received: May 11, 2007 / Revised version: June 20, 2007

Abstract Optical techniques are finding widespread use in analytical chemistry for chemical and bio-chemical analysis. During the past decade, there has been an increasing emphasis on miniaturization of chemical analysis systems and naturally this has stimulated a large effort in integrating microfluidics and optics in lab-on-a-chip microsystems. This development is partly defining the emerging field of optofluidics. Scaling analysis and experiments have demonstrated the advantage of micro-scale devices over their macroscopic counterparts for a number of chemical applications. However, from an optical point of view, miniaturized devices suffer dramatically from the reduced optical path compared to macroscale experiments, e.g. in a cuvette. Obviously, the reduced optical path complicates the application of optical techniques in lab-on-a-chip systems. In this paper we theoretically discuss how a strongly dispersive photonic crystal environment may be used to enhance the light-matter interactions, thus potentially compensating for the reduced optical path in lab-on-a-chip systems. Combining electromagnetic perturbation theory with full-wave electromagnetic simulations we address the prospects for achieving slow-light enhancement of Beer–Lambert–Bouguer absorption, photonic band-gap based refractometry, and high- Q cavity sensing.

1 Introduction

Optofluidics is a new branch within photonics which attempts to unify concepts from optics and microfluidics [1,2]. The purpose of having these two fields play in concert is at least twofold;

- i) Optofluidics may provide new means for doing optics, including fluidic tuning of optics [3,4,5,6].

- ii) Optofluidics may find widespread applications in lab-on-a-chip systems [7,8,9,10] and analytical chemistry in general, where optical techniques are being frequently used for chemical and bio-chemical analysis [11].

The increasing awareness from the lab-on-a-chip community of optofluidics is to a large extent driven by the past decade's emphasis on miniaturization of chemical analysis systems [12] which has naturally stimulated a large effort in integrating microfluidics [13,14] and optics in lab-on-a-chip microsystems [7,8]. While a broad variety of phenomena, properties, and applications benefit from the down-scaling in size [12], the conditions for optical sensing and detection are impeded tremendously by the reduced optical path length in lab-on-a-chip systems. Panel (b) in Fig. 1 illustrates a typical lab-on-a-chip implementation of an absorbance cell. The optical path length L is often reduced by several orders of mag-

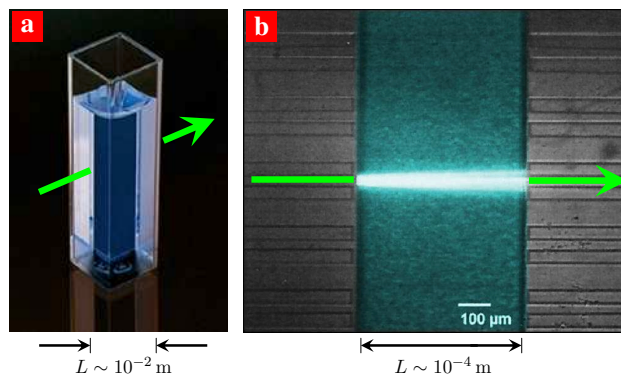


Fig. 1 Panel (a) illustrates a typical macroscopic cuvette while panel (b) shows a microscope image (top-view) of an equivalent lab-on-a-chip implementation of a microfluidic channel (vertical direction) integrated with planar optical waveguides (horizontal direction). Courtesy of K. B. Mogensen and J. P. Kutter (MIC – Department of Micro and Nanotechnology, Technical University of Denmark, www.mic.dtu.dk/microTAS).

* Invited paper for the "Optofluidics" special issue edited by Prof. David Erickson.

nitude compared to typical macroscopic counterparts, such as the cuvette shown in panel (a). A typical size reduction by two orders of magnitude will penalize the optical sensitivity in an inversely proportional manner, e.g. in a quantitative concentration measurement the lowest detectable chemical concentration will be increased by the same order of magnitude [15].

The above problem may conveniently be explained by the reduced light-matter interaction time τ given by the Wigner–Smith delay time. For a homogeneous system of length L we have

$$\tau \sim L/c, \quad (1)$$

with c being the speed of light. For small systems the photons will thus eventually have too little time for interacting with the chemical species and only very high concentrations can be quantified. Many applications involve *i*) minute sample volumes containing *ii*) very low concentrations of e.g. bio-molecules. There is thus obviously a strong call for miniaturized systems acknowledging the former without jeopardizing optical approaches quantifying the latter. In this work we explore the use of photonic crystal concepts for such a purpose.

Photonic crystals [16,17] constitute a class of artificial electromagnetic structures offering highly engineered dispersion properties not offered to us by any elements of Nature herself. Photonic crystals are porous structures, but with the voids arranged in a highly regular way, see Fig. 2). This makes electromagnetic radiation interact strongly with the matter for wavelengths λ comparable to the periodicity Λ of the photonic crystal. Photonic crystals are strongly dispersive environments supporting a number of phenomena including photonic band gaps and slow-light propagation [18,19]. As we shall see, liquid-infiltrated photonic crystals will overall inherit the unusual dispersion properties from their non-infiltrated counterparts, thus also changing the way light interacts with bio-molecules dissolved in the liquid. The effects can be quite spectacular compared to light-matter interactions in a spatially homogeneous liquid environment.

Previous experimental work on liquid-infiltrated photonic crystals may roughly be classified as studies emphasizing either fluidic tuning of optical properties [3, 20] or work focusing on optical sensing in fluidic environments [10, 21, 22, 23, 24, 25, 26, 27, 28]. On the theoretical side there has also recently been a considerable attention to tuning [29] and sensing aspects [30, 31, 32, 33, 34, 35, 36]. In passing, we note that somewhat parallel to the above development there has been an effort in fluidic tuning of photonic crystal fibers [37, 38, 39] and microstructured fibers have recently been integrated in lab-on-a-chip systems for sensing applications [40]. Finally, infiltrating with liquid crystals [41] seems to be an interesting direction for dynamically tunable photonic crystals [42] and photonic crystal fiber devices [43].

In this paper we outline our recent theoretical and numerical work [33, 34, 35, 36] on liquid-infiltrated pho-

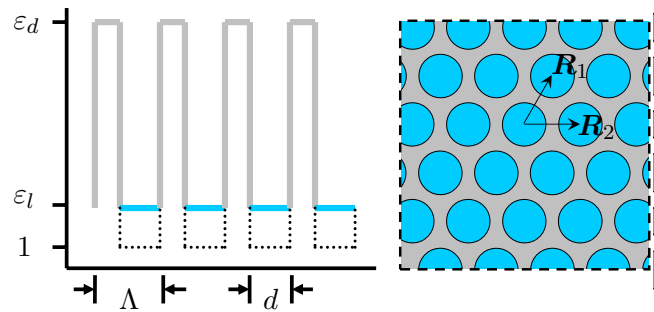


Fig. 2 Schematic of the dielectric function variations in a photonic crystal. High-index material with dielectric function ε_d is shown in gray while the liquid with dielectric function ε_l is indicated by blue coloring. The dashed curve indicates the dielectric function variation in the absence of liquid.

tonic crystals including potential applications for enhanced light-matter interactions in lab-on-a-chip systems. The remaining parts of the paper are organized as follows: in Sec. 2 we introduce our theoretical formalism, in Sec. 3 we address the dielectric properties of physiological liquids, in Sec. 4 we discuss general aspects of modes in liquid-infiltrated photonic crystals, and in Sec. 5 we give examples of potential applications in optical sensing. Finally, in Sec. 6 a discussion and conclusions are given.

2 Formalism

We consider photonic crystals made from a single high-index material (with dielectric function ε_d) which can be of either void-like or pillar-like nature. By infiltrating the photonic crystal by a liquid (with dielectric function $\varepsilon_l = n_l^2$) we have a spatially dependent dielectric function

$$\varepsilon(\mathbf{r}) = \begin{cases} \varepsilon_d, & \mathbf{r} \in \mathcal{V}_d, \\ \varepsilon_l, & \mathbf{r} \in \mathcal{V}_l, \end{cases} \quad (2)$$

where \mathcal{V}_d and \mathcal{V}_l are the domains of dielectric material and liquid, respectively. Fig. 2 illustrates an example of a planar photonic crystal and also indicates how the dielectric function changes upon liquid infiltration.

2.1 The wave equation

For the dielectric problem constituted by Eq. (2), the Maxwell equations lead to the following generalized eigenvalue problem for an electrical field with a harmonic time dependence [18,19]

$$\nabla \times \nabla \times |\mathbf{E}_m\rangle = \varepsilon \frac{\omega_m^2}{c^2} |\mathbf{E}_m\rangle \quad (3)$$

with ω_m being the angular eigenfrequency of the m th eigenfield $|\mathbf{E}_m\rangle$. We have for simplicity suppressed the spatial dependence of the dielectric function $\varepsilon(\mathbf{r})$. Since

the eigenvalue problem is of the generalized form, the eigenfields are orthonormal in the sense that

$$\langle \mathbf{E}_n | \varepsilon | \mathbf{E}_m \rangle = \delta_{nm} \quad (4)$$

where we have used the Dirac bra-ket notation with inner products between functions g and h defined according to

$$\langle g | h \rangle = \int d\mathbf{r} g^*(\mathbf{r})h(\mathbf{r}) \quad (5)$$

with the integral extending over all space unless otherwise indicated.

2.2 Bloch modes of photonic crystals

For a photonic crystal the dielectric function ε of Eq. (2) is periodic in space, i.e. $\varepsilon(\mathbf{r} + \mathbf{R}) = \varepsilon(\mathbf{r})$ with \mathbf{R} being a lattice vector, see Fig. 2. The solutions to Eq. (3) are in this case known as Bloch modes [18, 19] and are characterized by both a mode index m and a Bloch wave vector $\boldsymbol{\kappa}$. Introducing the explicit time and space dependencies we have

$$|\mathbf{E}_{m,\boldsymbol{\kappa}}(\mathbf{r}, t)\rangle = \exp[i(\boldsymbol{\kappa} \cdot \mathbf{r} - \omega_m t)] |\mathbf{E}_{m,\boldsymbol{\kappa}}(\mathbf{r})\rangle \quad (6)$$

where we have introduced the Bloch function $|\mathbf{E}_{m,\boldsymbol{\kappa}}(\mathbf{r})\rangle$ which inherits the periodicity of $\varepsilon(\mathbf{r})$. Typically, one has to rely on numerical approaches to the calculation of the Bloch modes of Eq. (3) in a photonic crystal. For this purpose we in this work employ a plane-wave expansion method with periodic boundary conditions [44] yielding the dispersion relation $\omega_m(\boldsymbol{\kappa})$. In general, the dispersion in a photonic crystal differs significantly from the free-space dispersion relation $\omega(\mathbf{k}) = ck$.

2.3 Perturbation theory

Many aspects of sensing will be adequately addressed with the aid of perturbation theory and in the following we briefly outline the basic equations of first-order electromagnetic perturbation theory. We assume we make a small frequency-independent perturbation $\Delta\varepsilon$ to the dielectric function, i.e.

$$\varepsilon \rightarrow \varepsilon + \Delta\varepsilon + \dots \quad (7a)$$

The perturbation is small in the sense that $\Delta\varepsilon \ll \varepsilon$ and we would like to know how this is going to change the eigenfrequencies and eigenfields. Expanding the frequency and the field in a similar manner

$$\omega \rightarrow \omega + \Delta\omega + \dots \quad (7b)$$

$$|\mathbf{E}\rangle \rightarrow |\mathbf{E}\rangle + |\Delta\mathbf{E}\rangle + \dots \quad (7c)$$

and substituting into the wave equation, Eq. (3), we may group terms according to the order of the correction. To

lowest order in the perturbation we arrive at the standard result that fields remain unchanged while the eigenfrequencies shift according to

$$\Delta\omega_m = -\frac{\omega_m}{2} \frac{\langle \mathbf{E}_m | \Delta\varepsilon | \mathbf{E}_m \rangle}{\langle \mathbf{E}_m | \varepsilon | \mathbf{E}_m \rangle}. \quad (8)$$

For the applications that we have in mind the perturbation will typically be caused by chemical changes or reactions in the liquid, i.e. the perturbation will be non-zero in the liquid part of space only. Thus, in general we will encounter problems with $\Delta\omega_m \propto f_m$ where

$$f_m \equiv \frac{\langle \mathbf{E}_m | \varepsilon | \mathbf{E}_m \rangle_{\mathcal{V}_l}}{\langle \mathbf{E}_m | \varepsilon | \mathbf{E}_m \rangle_{\mathcal{V}_{l+d}}} = \frac{\langle \mathbf{E}_m | \mathbf{D}_m \rangle_{\mathcal{V}_l}}{\langle \mathbf{E}_m | \mathbf{D}_m \rangle_{\mathcal{V}_{l+d}}} \quad (9)$$

is the filling fraction quantifying the relative optical overlap with the liquid, i.e. $0 \leq f \leq 1$. In the second equality of Eq. (9) we have introduced the displacement field $|\mathbf{D}\rangle = \varepsilon|\mathbf{E}\rangle$. The subscripts on the inner products emphasize the spatial domain of integration in Eq. (5). Note that compared to the definition normally used by the photonic crystal community [18] our definition quantifies the relative overlap with the liquid-part of space rather than the dielectric part given by $1 - f$ as easily seen from Eq. (4).

For a fixed frequency the result of the perturbation may alternatively be viewed as a shift $\Delta\boldsymbol{\kappa}$ in the Bloch wave vector $\boldsymbol{\kappa}$. Mathematically, the shift is calculated via the chain-rule

$$\Delta\boldsymbol{\kappa}_m = \left(\frac{\partial\omega_m}{\partial\boldsymbol{\kappa}} \right)^{-1} \Delta\omega_m = \frac{\omega_m}{2} \frac{\Delta\varepsilon_l}{\varepsilon_l} \frac{f_m}{\mathbf{v}_{g,m}} \quad (10)$$

where $\mathbf{v}_{g,m} = \partial\omega_m/\partial\boldsymbol{\kappa}$ is the group velocity of the m th mode.

In general, for enhanced light-matter interaction phenomena there is a balance between *i*) modifying the dispersion (compared to propagation through the homogeneous liquid) and *ii*) still maintaining a reasonable optical overlap with the liquid, i.e. keeping f of the order unity rather than close to zero.

3 Dielectric properties of physiological liquids

In this work we emphasize applications involving physiological liquids as can be found in biological systems. At low frequencies water is highly polarizable because of the polar nature of the H_2O molecules. In the static limit the relative dielectric function is around $\varepsilon \sim 80$. However, at optical frequencies the polar molecules move too slowly in respond to the temporally rapidly varying field and water becomes transparent to visible and infrared radiation. The dielectric function is typically of the order $\varepsilon \sim (1.33)^2 \simeq 1.8$. Compared to highly purified distilled water, physiological liquids have natural contents of various salts in dissolved form. One example

could be potassium chloride (KCl) which has a high solubility in water. The potassium (K^+) and chlorine (Cl^-) ions are highly mobile in water with a mobility around $\mu_{ion} \sim 10^{-7} m^2(Vs)^{-1}$. For ions carrying a charge Ze the ionic conductivity is given by

$$\sigma = ZeC_{ion}\mu_{ion} \quad (11)$$

where c_{ion} is the ionic concentration. Typically, the ionic concentration is of the order $c_{ion} \sim 1$ mM yielding conductivities of the order $\sigma_{ion} \sim 10^{-3} S/m$ [45]. The electrical field will induce a current density $\mathbf{J} = \sigma\mathbf{E}$ in the liquid, but from an optical point of view the form of Eq. (3) is formally retained, but now with a complex valued dielectric function

$$\varepsilon_l \rightarrow \varepsilon_l + i\frac{\sigma}{\omega}. \quad (12)$$

Consequences of the imaginary part were discussed in Ref. [34]. We here emphasize the quite similar form of Eq. (12) to the Drude model often employed for the response of metals at optical frequencies. For a liquid it will be an adequate description of its bulk properties, thus neglecting any surface chemistry as well as Debye-layer ion accumulation at the interfaces to other materials such as the high-index material forming the photonic crystal. Another issue could be electro-hydrodynamic phenomena where momentum is transferred from the ionic motion to the fluid (see e.g. Ref. [46] and references therein), but at optical frequencies such phenomena are strongly suppressed, since the Debye screening layer forms too slowly in response to the rapidly varying electrical field. It is common to introduce the Debye response time

$$\tau_D = \omega_D^{-1} = \varepsilon_l/\sigma \quad (13)$$

and for typical electrolytes, τ_D is of the order a micro second corresponding to a Debye frequency in the megahertz regime. For optical frequencies, $\omega \gg \omega_D$, it is thus fully adequate to treat the Ohmic damping due to the imaginary part in Eq. (12) perturbatively. The damping is given by $\alpha_m = 2\text{Im}\{\kappa_m\}$ which from Eq. (10) becomes

$$\alpha_m^{ion} = f_m \times \frac{\omega_D}{v_{g,m}}. \quad (14)$$

The attenuation will thus quite intuitively increase with a slowing down of the electromagnetic mode near photonic-band edges. Modes with a large optical overlap with the liquid of course suffer most from Ohmic dissipation as reflected by the proportionality of α to f . In a spatially homogenous liquid, Eq. (14) with $f = 1$ results in a damping of the order ω_D/c corresponding to a typical decay length of the order 1 m. For applications of liquid-infiltrated photonic crystals in lab-on-a-chip applications it thus seems adequate to treat typical physiological liquids and the high-index dielectric material at an equal footing, *i.e.* both materials are to a first approximation assumed lossless.

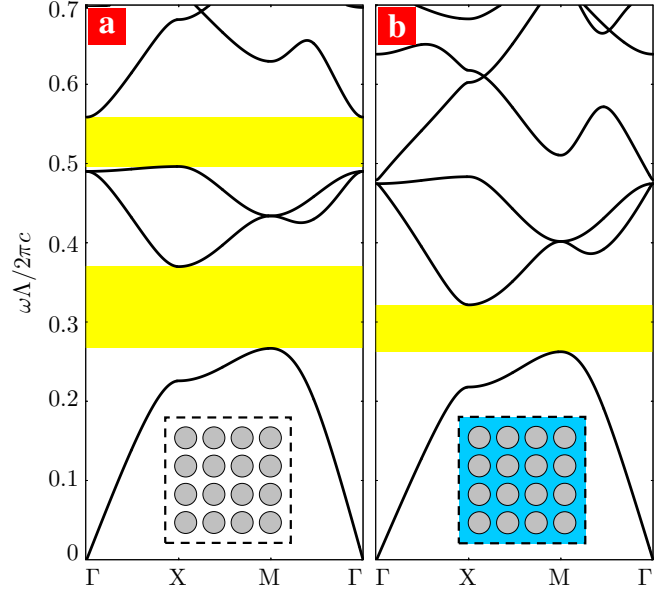


Fig. 3 TM modes for a square-lattice of pillars with diameter $d/\Lambda = 0.5$ and dielectric function $\varepsilon_d = 10.5$. Panel (a) shows results for the non-infiltrated photonic crystal and panel (b) is for the same photonic crystal infiltrated by a liquid with dielectric function $\varepsilon_l = (1.33)^2$.

4 Classification of photonic bands

The majority of experimental work on liquid-infiltrated photonic crystals has so far emphasized void-like structures. The pillar-like structures may be viewed as the geometrical inverse with the high and low-index materials being swapped. From Babinet's principle [47] one might

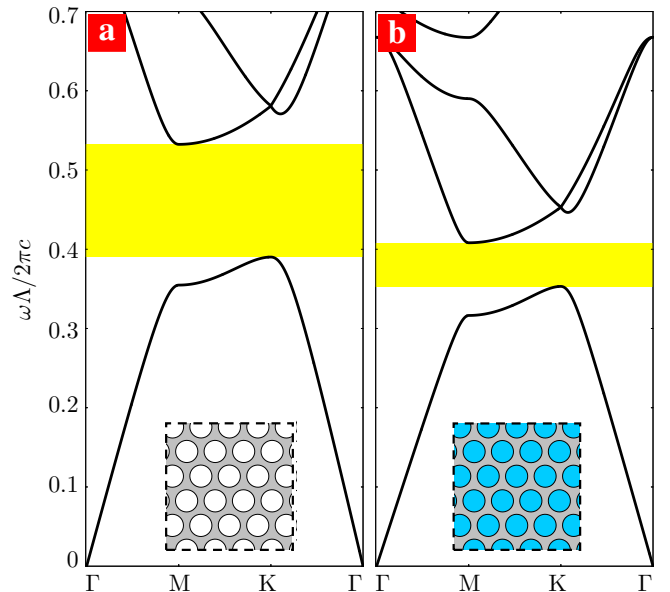


Fig. 4 TE modes for a triangular-lattice of voids with diameter $d/\Lambda = 0.96$ in a dielectric material with $\varepsilon_d = 10.5$. Panel (a) shows results for the non-infiltrated photonic crystal and panel (b) is for the same photonic crystal infiltration by a liquid with dielectric function $\varepsilon_l = (1.33)^2$.

imagine the two types of photonic crystals to have somewhat related properties. However, the source of formation of photonic band gaps are quite different in nature; for void-like structures the band-gaps arise from multiple reflections, i.e. Bragg scattering while band-gaps relate to Mie resonances for pillar-like structures [48, 49]. The sensitivity to infiltration by liquids is also somewhat different in terms of polarization. The discussion of dielectric versus air bands in Ref. [18] is naturally extended to the present context where we will refer to the bands as dielectric or liquid bands. Fig. 3 illustrates the typical TM properties of a square-lattice pillar-like structure. The band structure has been obtained with the aid of a plane-wave simulation [44]. The lowest band is obviously a dielectric band with $f \sim 0$ as clearly seen by the modest change upon infiltration. The second band is on the contrary a liquid band and the higher value of f causes a pronounced frequency shift of the upper band-gap edge upon infiltration by the liquid. Due to the reduced index contrast, especially high-order band-gaps may close upon liquid infiltration as seen by comparing panels (a) and (b) in Fig. 3.

Typical TE properties of a triangular-lattice void-like structure is illustrated in Fig. 4. The band structure has been obtained with the aid of a plane-wave simulation [44]. Again, the lowest band is predominantly a dielectric band with $f \sim 0.4$ as clearly seen by the modest change upon infiltration, though this is not as pronounced as for the pillar-like structure in Fig. 3. Likewise, the second band is a liquid band with a high value

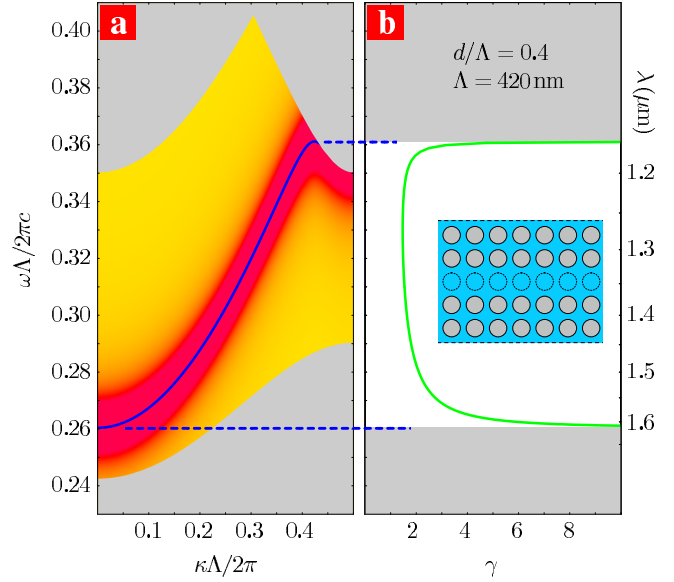


Fig. 6 Slow-light enhanced absorbance. Panel (a) shows the band structure for propagation of TM polarized light along the ΓX direction in a line-defect waveguide in a square lattice of period Λ with dielectric rods of diameter $d = 0.4\Lambda$ and $\varepsilon = 10.5$ with the structure infiltrated by a liquid with $\varepsilon = (1.33)^2$. The complete photonic band gap of the photonic crystal is indicated by yellow shading while grey shading indicates the finite density-of-states in the photonic crystal due to the projected bands in the Brillouin zone. Panel (b) shows the corresponding enhancement factor γ which exceeds unity over the entire bandwidth. The right y -axis shows the results in terms of the free-space wavelength when results are scaled to a structure with $\Lambda = 420$ nm.

of f causing a pronounced shift of the upper band-gap edge upon infiltration by the liquid.

Modes with a liquid-band behavior are of course of primary interest since the high electrical field intensity in the liquid allows for optofluidic tuning of the dispersion or likewise highly sensitive optical monitoring of chemical changes in the fluid. Fig. 5 shows results for the filling fraction f along with field-intensity plots for the dielectric and liquid bands associated with the band structures in panels (b) of Figs. 3 and 4. High values of f correlates with a pronounced field localization in the liquid while low values is associated with a marked field overlap with the dielectric.

5 Applications in sensing and quantitative analysis

5.1 Beer–Lambert–Bouguer absorption

The Beer–Lambert–Bouguer absorbance technique was developed two centuries ago and has since then become one of the classical optical workhorses in analytical chemistry [11]. The basic principle of an absorbance measurement is illustrated in Fig. 1. The optical probe, with

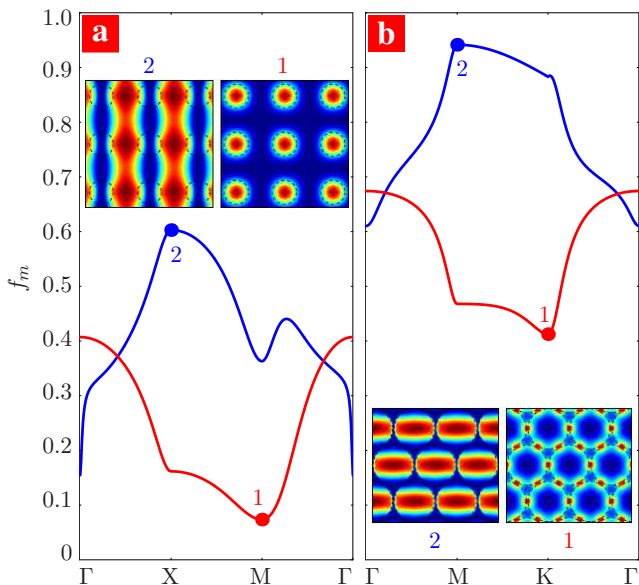


Fig. 5 Filling fraction for first dielectric (red line) and liquid (blue line) bands. Panel (a) shows results corresponding to the band structure in panel (b) of Fig. 3 while panel (b) shows results corresponding to panel (b) of Fig. 4. The insets show the electrical field intensity $|\mathbf{E}|^2$ at various high-symmetry points for the two types of bands.

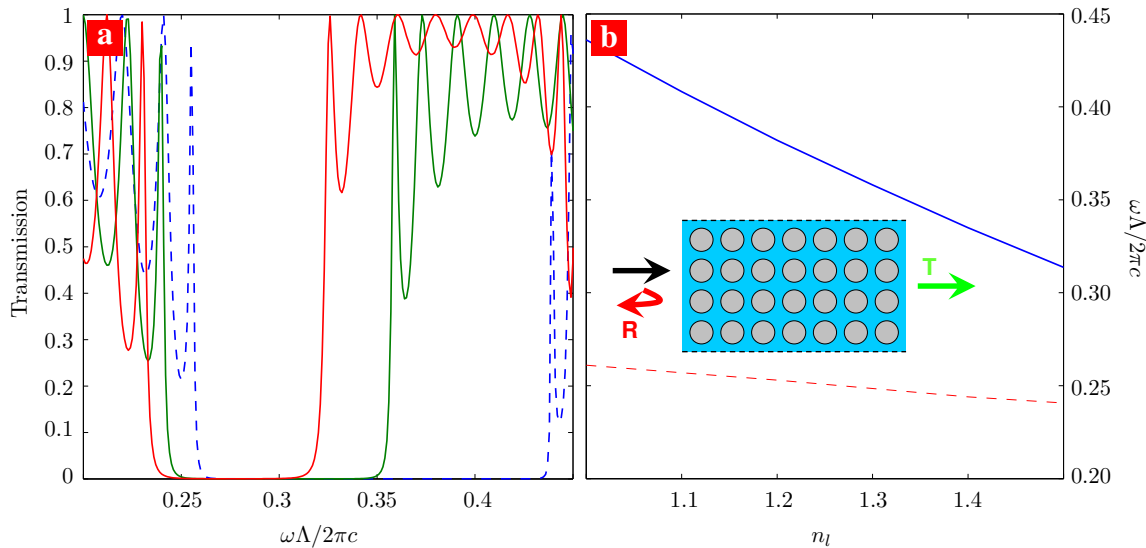


Fig. 7 Transmission of TM polarized light incident on a liquid-infiltrated photonic crystal based on a square-lattice of pillars with diameter $d/\Lambda = 0.4$ and dielectric function $\epsilon_d = 10.5$. Panel (a) shows the spectral transmission for the non-infiltrated photonic crystal (dashed line) and when infiltrated with a liquid with $n_l = 1.33$ (solid green line) and $n_l = 1.5$ (solid red line), respectively. Panel (b) shows the spectral shift of the upper (solid line) and lower (dashed line) transmission band edges for varying values of the liquid refractive index n_l .

intensity I_0 , is incident on a liquid sample with absorption parameter α_l reflecting a certain concentration C of some chemical species to be quantified. Typically the chemicals will be dissolved in a liquid, but for certain applications gas and even transparent solid phases are in principle also possible. To lowest order in the concentration we have

$$\alpha_l = \sum_i \eta_i C_i, \quad (15)$$

with the C_i being the concentration of the absorbing bio-molecules of the i th type with molar extinction coefficient η_i .

If we neglect coupling issues, the transmitted intensity I will then, quite intuitively, be exponentially damped,

$$I = I_0 \exp(-\gamma \alpha_l L). \quad (16)$$

We have, by hand, introduced γ as a dimensionless measure of possible dispersion enhanced light-matter interactions. For a uniform medium we of course have $\gamma \equiv 1$ and the expression then often goes under the name of Beer's law. For a dilute solution α_l correlates linearly with the concentration of the absorbing chemical species and Beer's law then provides simple optical means for detecting and quantifying the concentration of chemical solutions [11]. Evidently, the effect relies heavily on having a sufficiently long optical path length and the longer L is the lower a concentration can be monitored for a given sensitivity of the optical equipment measuring I/I_0 . Quite obviously, lab-on-a-chip implementations of chemical absorbance cells are facing major challenges due to the miniaturization as exemplified by recent experimental work by Mogensen *et al.* [15]. Here, we outline our recent suggestion to use slow-light phenomena

to compensate for the reduced optical path length [35]. In order to rigorously derive the enhancement factor γ for a liquid-infiltrated photonic crystal we apply perturbation theory, Eq. (10), to the problem of a small imaginary part $i\Delta\epsilon_l$ in the liquid. Comparing the corresponding damping $\alpha_m = 2\text{Im}\{\kappa_m\}$ to the damping in a spatially homogenous liquid, obtained from Eq. (10) with $f = 1$ and $v_g = c/n_l$, we arrive at an enhancement factor $\gamma_m \equiv \alpha_m/\alpha_l$ given by

$$\gamma_m = f_m \times \frac{c/n_l}{v_{g,m}}. \quad (17)$$

The interpretation of this result is straightforward; slow-light propagation, $v_g \ll c$, will significantly enhance the absorbance. The presence of the filling factor f is also quite obvious since only the relative fraction of the intensity residing in the liquid will contribute to the absorption. Finally, we note that for a spatially homogeneous liquid we get $\gamma = 1$ as required by the definition in Eq. (16). In general, the enhancement factor has a lower bound, $\gamma \geq 0$, while there is in principal no upper bound since the inverse group velocity diverges for Bloch wave vectors near the Brillouin zone (such as the X or M points) or near the center of the zone (the Γ point), see Fig. 3. In Fig. 6 we show results for a line-defect waveguide in a square lattice of period Λ with dielectric rods of diameter $d = 0.4\Lambda$ and $\epsilon = 10.5$. As expected, the pillar-like structure supports a mode with a very high optical overlap with the liquid, $f \sim 1$, combined with a reduced group velocity over the entire band width of the waveguide transmission window, see panel (a). Furthermore, at the Γ point the inverse group-velocity diverges

which is also the case near the upper waveguide transmission edge. In fact, the enhancement factor is of the order or larger than 2 over the entire bandwidth. Enhancement by an order of magnitude is easily achieved near the transmission band edges.

5.2 Refractometry

Refractometry in its basic form is another widely used method which most often is a qualitative measurement indicating chemical changes contrary to e.g. absorbance measurements which are of quantitative nature. Chemical reactions and changes most often cause a modification Δn_l of the refractive index, thus altering the optical response of e.g. a reflection or transmission measurement. Chemical changes may thus be monitored by watching the spectral shifts of e.g. transmission resonances [33,36]. Obviously, the larger a spectral shift the more sensitive is the method. As for the previous problem we will apply perturbation theory to study the spectral sensitivity due to a small perturbation $\Delta \varepsilon_l \simeq 2n_l \Delta n_l$. From Eq. (8) we get

$$\frac{\Delta \omega_m}{\omega_m} = -f_m \times \frac{\Delta \varepsilon_l}{2\varepsilon_l} \quad (18)$$

or introducing the free-space wavelength $\lambda = 2\pi c/\omega$ we may express the sensitivity in the form of a wavelength shift $\Delta \lambda$ due to a shift in liquid refractive index Δn_l ,

$$\frac{\Delta \lambda_m}{\Delta n_l} = f_m \times \frac{\lambda_m}{n_l}. \quad (19)$$

The interpretation is again quite intuitive. In a homogeneous liquid we have a dispersion $1/\lambda \propto \omega(\boldsymbol{\kappa}) = (c/n_l)k$ so that $\Delta \lambda/\Delta n_l = \lambda/n_l$ which is obviously the ultimate sensitivity one can have. However, transmission through homogenous media is not associated with any pronounced resonances or cut-offs. Transmission experiments reflect the photonic density-of-states and strong resonances may be achieved by infiltrating a photonic crystal with the liquid [34]. In that case the sensitivity is naturally corrected by the filling factor f as shown by the rigorous perturbative analysis in Eq. (19). From Eq. (19) the working wavelength is of course important to the sensitivity. However, this is a somewhat trivial effect for refractometry in general, while the dependence on filling fraction in Eq. (19) is really the limiting factor. The performance of different structures, ranging from evanescent field sensing devices to liquid-infiltrated photonic crystals, may thus be compared by comparing the corresponding filling fractions. Such relative comparisons has previously been suggested in the literature [30], but Eq. (19) does in fact allow for an absolute definition of the sensitivity.

Evanescent field-sensing devices are characterized by an almost vanishing f which will typically only be of the order a few percent. Depending on the design, void-like

photonic crystals offer moderate-to-high filling fractions depending on the void-to-solid volume ratio, and similarly for pillar-like photonic crystals.

Figure 7 shows a proposal of refractometry with a liquid-infiltrated photonic crystal. The simple structure consists of a square-lattice of pillars with diameter $d/\Lambda = 0.4$ and dielectric function $\varepsilon_d = 10.5$. Transmission spectra for TM polarized light have been obtained by means of a two-dimensional finite-difference time-domain (FDTD) method, see Ref. [33] and references therein. Panel (a) shows the spectral transmission for the non-infiltrated photonic crystal (dashed line) and when infiltrated with a liquid with $n_l = 1.33$ (solid green line) and $n_l = 1.5$ (solid red line), respectively. From the band structure in Fig. 3 one would expect a suppression of the transmission for frequencies inside the photonic band gap which correlates nicely with the observed transmission. Furthermore, when infiltrating the photonic crystal with liquid, the spectral position of the upper transmission band edge is expected to be more sensitive to the perturbation than the lower transmission band edge. Panel (b) shows the spectral shift of the upper and lower transmission band edges for varying values of the liquid refractive index n_l . The upper curve does indeed have a larger slope than the lower curve which according to Eq. (19) supports the picture of transmission through a liquid band and dielectric band, respectively. The transmission results agrees quantitatively with the band-structure theory as studied in detail in Ref. [33] and from Eq. (19) we estimate that $f \sim 80\%$ for the transmission through the liquid band.

In Fig. 8 we show another implementation of refractometry employing a liquid-infiltrated photonic crystals wave-guide structure based on a triangular-lattice of voids with diameter $d/\Lambda = 0.6$ and dielectric function $\varepsilon_d = 10.5$. Selective filling of the defect wave-guide structure is of course crucial, but nanofluidic tuning has recently been demonstrated experimentally in a similar structure [3]. Panel (a) shows the spectral transmission of TE polarized light for the non-infiltrated photonic crystal (dashed line) and when infiltrated with a liquid with $n_l = 1.33$ (solid green line) and $n_l = 1.5$ (solid red line), respectively. Panel (b) shows the spectral shift of the upper and lower transmission band edges for varying values of the liquid refractive index n_l . Again, the upper curve corresponds to transmission through a band of predominantly liquid-band nature with $f \sim 40\%$ estimated from Eq. (19).

Above we have emphasized transmission properties, but spectral shifts could alternatively be monitored in a reflection configuration.

5.3 Cavity based sensing

Obviously, cavity modes may be used for refractometry where Eq. (19) also applies. Defect structures in photonic crystals are quite interesting in this context and

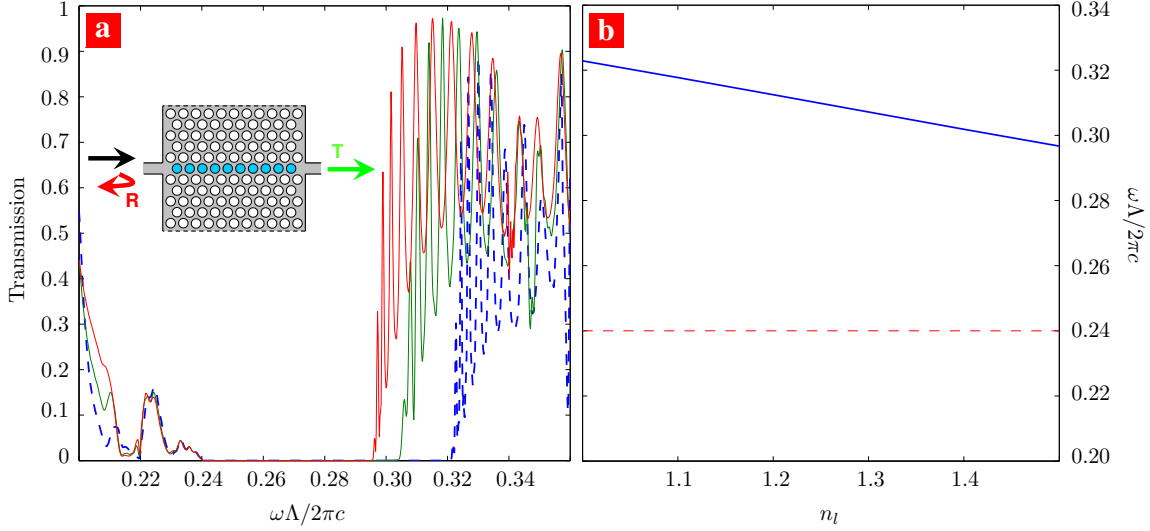


Fig. 8 Transmission of TE polarized light incident on a liquid-infiltrated photonic crystals wave-guide structure based on a triangular-lattice of voids with diameter $d/\Lambda = 0.6$ and dielectric function $\varepsilon_d = 10.5$. Panel (a) shows the spectral transmission for the non-infiltrated photonic crystal (dashed line) and when infiltrated with a liquid with $n_l = 1.33$ (solid green line) and $n_l = 1.5$ (solid red line), respectively. Panel (b) shows the spectral shift of the upper (solid line) and lower (dashed line) transmission band edges for varying values of the liquid refractive index n_l .

in recent experiments Chow *et al.* have pursued this direction [23]. For refractometric applications the quality factor Q of a resonance should be sufficiently high to easily monitor and resolve even small spectral shifts of the resonance. Here, we would like to emphasize another potential usage of high- Q resonators somewhat resembling the Beer–Lambert–Bouguer absorption technique. For the slow-light enhancement we note that the divergence of the inverse group velocity near the edge of the Brillouin zone is basically a standing wave phenomenon. Thus, cavity modes may in a similar way be used to enhance the light-matter interaction time τ , but contrary to the case of Eq. (1) the Wigner–Smith delay time now relates to the cavity quality factor Q . In the following we consider an isolated Lorentzian resonance,

$$\rho_m(\omega) = -\frac{1}{\pi} \text{Im} \left\{ \frac{1}{\omega - \omega_m + i\Gamma_m/2} \right\}, \quad (20)$$

with the line width Γ_m corresponding to an intrinsic quality factor $Q_{\text{in}} = \omega_m/\Gamma_m$. We imagine that the intrinsic quality factor includes everything but the broadening due to absorption caused by the presence of bio-molecules in the liquid. The total quality factor Q may then be written as

$$Q = (Q_{\text{in}}^{-1} + Q_{\text{abs}}^{-1})^{-1} \simeq \begin{cases} Q_{\text{abs}}, & Q_{\text{abs}} \ll Q_{\text{in}}, \\ Q_{\text{in}}, & \alpha_l \rightarrow 0, \end{cases} \quad (21)$$

where Q_{abs} is the contribution from absorption. High- Q cavities would be of prime interest to sensing since the line width would be dominated by the presence of absorbing bio-molecules rather than the intrinsic line width associated with the localization of light. Obviously, the

higher a Q_{in} the lower a concentration of molecules can be detected. In order to quantify this further we consider the limit of weak absorption in the liquid and apply perturbation theory. Calculating the imaginary shift of ω_m due to $\Delta\varepsilon = i\Delta\varepsilon_l$ from Eq. (8) and substituting into Eq. (20) we identify an additional broadening corresponding to

$$Q_{\text{abs}} = f_m^{-1} \times \frac{2\pi n_l}{\alpha_l \lambda_m} \quad (22)$$

where we have introduced the absorption parameter α_l of the liquid. The form of Eq. (22) resembles the form derived for e.g. homogeneous micro-sphere resonators [50] except for the presence of the filling factor f . Obviously, the lower an overlap with the absorbing liquid the smaller an additional broadening of the intrinsic resonance line width.

If we consider just one type of molecules, see Eq. (15), the criterion in Eq. (21) means that the lowest detectable concentration is bound by

$$C \gtrsim f_m^{-1} \times \frac{1}{\eta \lambda_m Q_{\text{in}}} \quad (23)$$

with η being the molar extinction coefficient. As an example, for a typical value $\eta \sim 1 \text{ M}^{-1} \mu\text{m}^{-1}$ a detection in the micro-molar regime would require $f \times Q_{\text{in}} \gtrsim 10^5$.

Cavity designs optimizing the product $f \times Q_{\text{in}}$ are obviously needed, but it is also well-known that for slab-like photonic crystals the typical high- Q cavities will have a quite modest f to prevent degradation of Q by out-of-plane leakage [51,52] though some designs may get around this [53,54]. Indeed, the refractometric measurements in Ref. [23] suggest that $f \sim 20\%$ for their cavity mode with $Q \sim 400$. Cavities in three-dimensional

photonic crystals with photonic-band gap confinement in all three directions could be an interesting scenario. As an alternative, recent experiments with liquid microdroplets [55,56] facilitate whispering-gallery modes with $f \simeq 1$ and potentially the intrinsic Q -factor can be made very high due to the absence of surface roughness at the almost perfect liquid-air interface which is smooth on the molecular length scale. Ref. [56] reported $Q \sim 10^5$ in a fiber-coupled experiment. Experimentally one might use the above scheme to quantify concentrations e.g. by time resolved ring-down spectroscopy or by other means such as transmission experiments typically employed for characterization of high- Q resonators [57].

6 Conclusion

With the increasing emphasis on miniaturization of chemical analysis systems there is presently a strong effort devoted to integrating microfluidics and optics in lab-on-a-chip microsystems. We have outlined possible applications of optofluidics in this context and used simple theoretical approaches to illustrate how light-matter interactions may be enhanced in liquid-infiltrated photonic crystals supporting highly dispersive modes and pronounced resonances.

Our formalism combines electromagnetic perturbation theory with full-wave electromagnetic simulations. The latter is used in calculating the dispersion properties of ideal (lossless) liquid-infiltrated photonic crystals while the former is used systematically to predict the spectral effects and changes caused by chemical perturbations of the infiltrated liquid.

In this paper we implicitly focused on near-infrared wavelengths with values for the high-index material resembling silicon. However, we emphasize that the general concepts apply equally well to other wavelength regimes such as the visible regime as in Ref. [10] or even the terahertz regime emphasized in Refs. [26,30,31]. The phenomena that we have discussed do to some extent rely on a sufficient index contrast between the liquid and the high-index materials. While polymers are certainly attractive materials for future low-cost disposable lab-on-a-chip devices they might not provide a sufficient index contrast for all of the applications that we have discussed and the choice of wavelength and materials should of course reflect the particular applications in mind.

With this theoretical paper we have sought to emphasize the potential benefits from using liquid-infiltrated photonic crystals for sensing purposes in lab-on-a-chip systems such as label-free sensing of bio-molecules. While photonic crystal concepts are generally considered a promising route to highly sensitive devices, our theory clearly demonstrates an inevitable challenge; the photonic crystal design needs to balance between having a strong optical proximity from the photonic crystal structure and at the same time supporting a decent optical overlap with

the liquid. On the other hand, the huge design space offered by photonic crystals seems to allow us to explore and cope with this challenge. In conclusion we believe that photonic crystals may be used to facilitate enhanced light-matter interactions which may be traded for yet smaller miniaturized systems or for increased sensitivity of existing devices.

Acknowledgements We thank A. Kristensen, M. Gersborg-Hansen, J. P. Kutter, K. B. Mogensen, H. Bruus, and J. Lægsgaard for discussions. This work is financially supported by the *Danish Council for Strategic Research* through the *Strategic Program for Young Researchers* (grant no: 2117-05-0037).

References

1. Psaltis, D., Quake, S.R., Yang, C.H.: Developing optofluidic technology through the fusion of microfluidics and optics. *Nature* **442**(7101) (2006) 381 – 386
2. Monat, C., Domachuk, P., Eggleton, B.J.: Integrated optofluidics: A new river of light. *Nature Photonics* **1** (2007) 106 – 114
3. Erickson, D., Rockwood, T., Emery, T., Scherer, A., Psaltis, D.: Nanofluidic tuning of photonic crystal circuits. *Opt. Lett.* **31**(1) (2006) 59 – 61
4. Diehl, L., Lee, B.G., Behroozi, P., Lončar, M., Belkin, M.A., Capasso, F., Aellen, T., Hofstetter, D., Beck, M., Faist, J.: Microfluidic tuning of distributed feedback quantum cascade lasers. *Opt. Express* **14**(24) (2006) 11660 – 11667
5. Levy, U., Campbell, K., Groisman, A., Mookherjea, S., Fainman, Y.: On-chip microfluidic tuning of an optical microring resonator. *Appl. Phys. Lett.* **88**(11) (2006) 111107
6. Gersborg-Hansen, M., Kristensen, A.: Tunability of optofluidic distributed feedback dye lasers. *Opt. Express* **15**(1) (2007) 137 – 142
7. Verpoorte, E.: Chip vision - optics for microchips. *Lab Chip* **3**(3) (2003) 42N – 52N
8. Mogensen, K.B., Klank, H., Kutter, J.P.: Recent developments in detection for microfluidic systems. *Electrophoresis* **25**(21-22) (2004) 3498 – 3512
9. Balslev, S., Jørgensen, A.M., Bilenberg, B., Mogensen, K.B., Snakenborg, D., Geschke, O., Kutter, J.P., Kristensen, A.: Lab-on-a-chip with integrated optical transducers. *Lab Chip* **6**(2) (2006) 213 – 217
10. Choi, C.J., Cunningham, B.T.: Single-step fabrication and characterization of photonic crystal biosensors with polymer microfluidic channels. *Lab Chip* **6**(10) (2006) 1373 – 1380
11. Skoog, D.A., West, D.M., Holler, F.J.: *Fundamentals of Analytical Chemistry*. Saunders College Publishing, New York (1997)
12. Janasek, D., Franzke, J., Manz, A.: Scaling and the design of miniaturized chemical-analysis systems. *Nature* **442**(7101) (2006) 374 – 380
13. Squires, T.M., Quake, S.R.: Microfluidics: Fluid physics at the nanoliter scale. *Rev. Mod. Phys.* **77** (2005) 977 – 1026

14. Whitesides, G.M.: The origins and the future of microfluidics. *Nature* **442**(7101) (2006) 368 – 373
15. Mogensen, K.B., El-Ali, J., Wolff, A., Kutter, J.P.: Integration of polymer waveguides for optical detection in microfabricated chemical analysis systems. *Appl. Optics* **42**(19) (2003) 4072 – 4079
16. Yablonovitch, E.: Inhibited spontaneous emission in solid state physics and electronics. *Phys. Rev. Lett.* **58**(20) (1987) 2059–2062
17. John, S.: Strong localization of photons in certain disordered dielectric superlattices. *Phys. Rev. Lett.* **58**(23) (1987) 2486 – 2489
18. Joannopoulos, J.D., Meade, R.D., Winn, J.N.: *Photonic crystals: molding the flow of light*. Princeton University Press, Princeton (1995)
19. Sakoda, K.: *Optical Properties of Photonic Crystals*. 2 edn. Volume 80 of Springer Series in Optical Sciences. Springer-Verlag, Berlin (2005)
20. Samakkulam, K., Sulkin, J., Giannopoulos, A., Choquette, K.D.: Micro-fluidic photonic crystal vertical cavity surface emitting laser. *Electron. Lett.* **42**(14) (2006) 809 – 811
21. Lončar, M., Scherer, A., Qiu, Y.M.: Photonic crystal laser sources for chemical detection. *Appl. Phys. Lett.* **82**(26) (2003) 4648 – 4650
22. Topol'ančik, J., Bhattacharya, P., Sabarinathan, J., Yu, P.C.: Fluid detection with photonic crystal-based multi-channel waveguides. *Appl. Phys. Lett.* **82**(8) (2003) 1143 – 1145
23. Chow, E., Grot, A., Mirkarimi, L.W., Sigalas, M., Girolami, G.: Ultracompact biochemical sensor built with two-dimensional photonic crystal microcavity. *Opt. Lett.* **29**(10) (2004) 1093 – 1095
24. Adams, M.L., Lončar, M., Scherer, A., Qiu, Y.M.: Microfluidic integration of porous photonic crystal nanolasers for chemical sensing. *IEEE J. Sel. Areas Commun.* **23**(7) (2005) 1348 – 1354
25. Chakravarty, S., Topol'ančik, J., Bhattacharya, P., Chakrabarti, S., Kang, Y., Meyerhoff, M.E.: Ion detection with photonic crystal microcavities. *Opt. Lett.* **30**(19) (2005) 2578 – 2580
26. Hasek, T., Kurt, H., Citrin, D.S., Koch, M.: Photonic crystals for fluid sensing in the subterahertz range. *Appl. Phys. Lett.* **89**(17) (2006) 173508
27. Skivesen, N., Têtu, A., Kristensen, M., Kjems, J., Frandsen, L.H., Borel, P.I.: Photonic-crystal waveguide biosensor. *Opt. Express* **15**(6) (2007) 3169 – 3176
28. Lee, M., Fauchet, P.M.: Two-dimensional silicon photonic crystal based biosensing platform for protein detection. *Opt. Express* **15**(8) (2007) 4530 – 4535
29. Sharkawy, A., Pustai, D., Shi, S.Y., Prather, D.W.: Modulating dispersion properties of low index photonic crystal structures using microfluidics. *Opt. Express* **13**(8) (2005) 2814 – 2827
30. Kurt, H., Citrin, D.S.: Coupled-resonator optical waveguides for biochemical sensing of nanoliter volumes of analyte in the terahertz region. *Appl. Phys. Lett.* **87**(24) (2005) 241119
31. Kurt, H., Citrin, D.S.: Photonic crystals for biochemical sensing in the terahertz region. *Appl. Phys. Lett.* **87**(4) (2005) 041108
32. Prasad, T., Mittleman, D.M., Colvin, V.L.: A photonic crystal sensor based on the superprism effect. *Opt. Mater.* **29**(1) (2006) 56 – 59
33. Xiao, S., Mortensen, N.A.: Highly dispersive photonic band-gap-edge optofluidic biosensors. *J. Eur. Opt. Soc., Rapid Publ.* **1** (2006) 06026
34. Mortensen, N.A., Ejsing, S., Xiao, S.: Liquid-infiltrated photonic crystals: Ohmic dissipation and broadening of modes. *J. Eur. Opt. Soc., Rapid Publ.* **1** (2006) 06032
35. Mortensen, N.A., Xiao, S.: Slow-light enhancement of beer-lambert-bouguer absorption. *Appl. Phys. Lett.* **90** (2007) 141108
36. Xiao, S., Mortensen, N.A.: Proposal of highly sensitive optofluidic biosensors based on dispersive photonic crystal waveguides. *J. Opt. A: Pure Appl. Opt.* **9** (2007) in press [arXiv:physics/0703063].
37. Mach, P., Dolinski, M., Baldwin, K.W., Rogers, J.A., Kerbage, C., Windeler, R.S., Eggleton, B.J.: Tunable microfluidic optical fiber. *Appl. Phys. Lett.* **80**(23) (2002) 4294 – 4296
38. Domachuk, P., Nguyen, H.C., Eggleton, B.J.: Transverse probed microfluidic switchable photonic crystal fiber devices. *IEEE Photonics Technol. Lett.* **16**(8) (2004) 1900 – 1902
39. Domachuk, P., Nguyen, H.C., Eggleton, B.J., Straub, M., Gu, M.: Microfluidic tunable photonic band-gap device. *Appl. Phys. Lett.* **84**(11) (2004) 1838 – 1840
40. Rindorf, L., Høiby, P.E., Jensen, J.B., Pedersen, L.H., Bang, O., Geschke, O.: Towards biochips using microstructured optical fiber sensors. *Anal. Bioanal. Chem.* **385**(8) (2006) 1370 – 1375
41. Yablonovitch, E.: Optics - liquid versus photonic crystals. *Nature* **401**(6753) (1999) 539 – +
42. Busch, K., John, S.: Liquid-crystal photonic-band-gap materials: The tunable electromagnetic vacuum. *Phys. Rev. Lett.* **83**(5) (1999) 967 – 970
43. Larsen, T.T., Bjarklev, A., Hermann, D.S., Broeng, J.: Optical devices based on liquid crystal photonic bandgap fibres. *Opt. Express* **11**(20) (2003) 2589 – 2596
44. Johnson, S.G., Joannopoulos, J.D.: Block-iterative frequency-domain methods for Maxwell's equations in a planewave basis. *Opt. Express* **8**(3) (2001) 173 – 190
45. Bruus, H.: *Theoretical Microfluidics*. 1 edn. Oxford University Press, Oxford (2007) in press.
46. Mortensen, N.A., Olesen, L.H., Belmon, L., Bruus, H.: Electrohydrodynamics of binary electrolytes driven by modulated surface potentials. *Phys. Rev. E* **71**(5) (2005) 056306
47. Born, M., Wolf, E.: *Principles of Optics*. 7 edn. Cambridge University Press, Cambridge, UK (1999)
48. Sigalas, M.M., Soukoulis, C.M., Chan, C.T., Turner, D.: Localization of electromagnetic waves in two-dimensional disordered systems. *Phys. Rev. B* **53**(13) (1996) 8340 – 8348
49. Lidorikis, E., Sigalas, M.M., Economou, E.N., Soukoulis, C.M.: Gap deformation and classical wave localization in disordered two-dimensional photonic-band-gap materials. *Phys. Rev. B* **61**(20) (2000) 13458 – 13464
50. Gorodetsky, M.L., Savchenkov, A.A., Ilchenko, V.S.: Ultimate Q of optical microsphere resonators. *Opt. Lett.* **21**(7) (1996) 453 – 455

51. Yoshie, T., Vučković, J., Scherer, A., Chen, H., Deppe, D.: High quality two-dimensional photonic crystal slab cavities. *Appl. Phys. Lett.* **79**(26) (2001) 4289 – 4291
52. Akahane, Y., Asano, T., Song, B.S., Noda, S.: High-Q photonic nanocavity in a two-dimensional photonic crystal. *Nature* **425**(6961) (2003) 944 – 947
53. Asano, T., Song, B.S., Akahane, Y., Noda, S.: Ultrahigh-Q nanocavities in two-dimensional photonic crystal slabs. *IEEE J. Sel. Top. Quantum Electron.* **12**(6) (2006) 1123 – 1134
54. Tomljenovic-Hanic, S., de Sterke, C.M., Steel, M.J.: Design of high-Q cavities in photonic crystal slab heterostructures by air-holes infiltration. *Opt. Express* **14**(25) (2006) 12451 – 12456
55. Azzouz, H., Alkhafadiji, L., Balslev, S., Johansson, J., Mortensen, N.A., Nilsson, S., Kristensen, A.: Levitated droplet dye laser. *Opt. Express* **14**(10) (2006) 4374 – 4379
56. Hossein-Zadeh, M., Vahala, K.J.: Fiber-taper coupling to whispering-gallery modes of fluidic resonators embedded in a liquid medium. *Opt. Express* **14**(22) (2006) 10800 – 10810
57. Vahala, K.J.: Optical microcavities. *Nature* **424**(6950) (2003) 839 – 846